Atmos. Chem. Phys., 21, 15431–15445, 2021
https://doi.org/10.5194/acp-21-15431-2021

Atmospheric Chemistry and Physics
Open Access
EGU

Aerosol transport pathways and source attribution in China during the COVID-19 outbreak

Lili Ren[1], Yang Yang[1], Hailong Wang[2], Pinya Wang[1], Lei Chen[1], Jia Zhu[1], and Hong Liao[1]

[1]Jiangsu Key Laboratory of Atmospheric Environment Monitoring and Pollution Control, Jiangsu Collaborative Innovation Center of Atmospheric Environment and Equipment Technology, School of Environmental Science and Engineering, Nanjing University of Information Science and Technology, Nanjing, Jiangsu, China
[2]Atmospheric Sciences and Global Change Division, Pacific Northwest National Laboratory, Richland, Washington, USA

Correspondence: Yang Yang (yang.yang@nuist.edu.cn)

Received: 16 April 2021 – Discussion started: 3 May 2021
Revised: 3 August 2021 – Accepted: 26 September 2021 – Published: 15 October 2021

Abstract. Due to the coronavirus disease 2019 (COVID-19) pandemic, human activities and industrial productions were strictly restricted during January–March 2020 in China. Despite the fact that anthropogenic aerosol emissions largely decreased, haze events still occurred. Characterization of aerosol transport pathways and attribution of aerosol sources from specific regions are beneficial to air quality and pandemic control strategies. This study establishes source–receptor relationships in various regions covering all of China during the COVID-19 outbreak based on the Community Atmosphere Model version 5 with Explicit Aerosol Source Tagging (CAM5-EAST). Our analysis shows that $PM_{2.5}$ burden over the North China Plain between 30 January and 19 February is mostly contributed by local emissions (40 %–66 %). For other regions in China, $PM_{2.5}$ burden is largely contributed from nonlocal sources. During the most polluted days of the COVID-19 outbreak, local emissions within the North China Plain and eastern China contributed 66 % and 87 % to the increase in surface $PM_{2.5}$ concentrations, respectively. This is associated with the anomalous mid-tropospheric high pressure at the location of the climatological East Asia trough and the consequently weakened winds in the lower troposphere, leading to the local aerosol accumulation. The emissions outside China, especially those from South Asia and Southeast Asia, contribute over 50 % to the increase in $PM_{2.5}$ concentration in southwestern China through transboundary transport during the most polluted day. As the reduction in emissions in the near future is desirable, aerosols from long-range transport and unfavorable meteorological conditions are increasingly important to regional air quality and need to be taken into account in clean-air plans.

1 Introduction

The coronavirus disease 2019 (COVID-19) has spread worldwide since December 2019 and resulted in more than a million cases within the first 4 months (Sharma et al., 2020; Dong et al., 2020). In order to curb the virus's spread among humans, measures were taken by the Chinese government on 23 January 2020 to minimize the interaction among people, including strict isolation, prohibition of large-scale private and public gatherings, restriction of private and public transportation, and even lockdown of cities (Tian et al., 2020; Wang et al., 2020). The estimated NO_x emissions in eastern China were reduced by 60 %–70 %, of which 70 %–80 % were related to the reduced road traffic and 20 %–25 % from industrial enterprises shutdown during the COVID-19 lockdown period. However, severe air pollution events still occurred in eastern China during the COVID-19 lockdown, even though the anthropogenic emissions were greatly reduced (Huang et al., 2020). The unprecedented large-scale restrictions resulting from the COVID-19 epidemic provide an opportunity to research the relationship between dramatic anthropogenic emission reductions and air quality changes (e.g., Bao et al., 2020; Li et al., 2020; Wang et al., 2020). Bao et al. (2020) reported that during the COVID-19 lockdown period the air quality index and the $PM_{2.5}$ (particulate matter less than 2.5 µm in diameter) concentration were de-

creased by 7.8 % and 5.9 % on average, respectively, in 44 cities in northern China, mainly due to travel restrictions. By applying the WRF-CAMx model together with air quality monitoring data, Li et al. (2020) revealed that although primary particle emissions were reduced by 15 %–61 % during the COVID-19 lockdown over the Yangtze River Delta region, the daily mean concentration of $PM_{2.5}$ was still relatively high, reaching up to 79 $\mu g\,m^{-3}$. Wang et al. (2020) found that the relative reduction in $PM_{2.5}$ precursors was twice as much as the reduction in $PM_{2.5}$ concentration, in part due to the unfavorable meteorological conditions during the COVID-19 outbreak in China that led to the formation of the heavy haze. Huang et al. (2020) and Le et al. (2020) reported that stagnant air conditions, high atmospheric humidity and enhanced atmospheric oxidizing capacity led to a severe haze event in northern China during the COVID-19 pandemic.

Aerosols are main air pollutants that play important roles in the atmosphere due to their adverse effects on air quality, visibility (Vautard et al., 2009; Watson, 2002), human health (Lelieveld et al., 2019; Heft-Neal et al., 2018), the Earth's energy balance, and regional and global climate (Ramanathan et al., 2001; Anderson et al., 2003; Yang et al., 2019a; Wang et al., 2020; Smith et al., 2020). With its rapid development in recent decades, China has experienced severe air pollution that damages human health and causes regional climate change (Chai et al., 2014; Liao et al., 2015; Fan et al., 2020). In order to control air pollution, the Chinese government issued and implemented the Air Pollution Prevention and Control Action Plan in 2013 (China State Council, 2013). Although emissions in China have decreased significantly in recent years (Zheng et al., 2018), aerosols transported from other source regions could add on top of local emissions (Yang et al., 2017a, 2018a; Ren et al., 2020). Therefore, it is important to understand the relative effects of local emissions and regional transport on aerosols in China.

Source tagging and apportionment is an effective way to establish aerosol source–receptor relationships, which is conducive to both scientific research and emission control strategies (Yu et al., 2012). By applying particulate source apportionment technology in the CAMx model, Xue et al. (2014) found that the contributions of regional transport to annual average $PM_{2.5}$ concentrations in Hainan, Shanghai, Jiangsu, Zhejiang, Jilin and Jiangxi provinces of China are more than 45 %. By adding a chemical tracer into the WRF model, Wang et al. (2016) studied the sources of black carbon (BC) aerosol in Beijing and reported that about half of BC in Beijing came from the central North China Plain. Liu et al. (2017) applied the WRF-Chem model and showed that Foshan, Guangzhou and Dongguan, with relatively high emissions, contributed 14 %, 13 % and 10 %, respectively, to the regional mean $PM_{2.5}$ concentration in the Pearl River Delta.

Previous studies only focused on regional transport of aerosols, and very few studies have explored the aerosol transport pathways and source attribution covering all of China during the COVID-19 pandemic. In this study, the global aerosol–climate model CAM5 (Community Atmosphere Model, version 5) equipped with explicit aerosol source tagging (CAM5-EAST) is employed to quantify source–receptor relationships and transport pathways of aerosols during the COVID-19 outbreak in China. We also provide model evaluations of $PM_{2.5}$ concentrations against observations made during the COVID-19 outbreak. With the aerosol source tagging technique, source region contributions to $PM_{2.5}$ column burden over various receptor regions and transport pathways in China are analyzed. The source contributions to the changes in near-surface $PM_{2.5}$ in the most polluted days compared to the monthly means during February 2020 are also quantified. Our study provides source apportionment of aerosols covering all of China and quantifies the contribution from foreign transport for the first time in the case of COVID-19 emission reductions, which is beneficial to the investigation of policy implications for future air pollution control.

2 Methods

2.1 Model description and experimental setup

The CAM5 model is applied to estimate the $PM_{2.5}$ changes during the COVID-19 period, which is the atmospheric component of the Earth system model CESM (Community Earth System Model, Hurrell et al., 2013). In this study, major aerosol species including sulfate, BC, primary organic matter (POM), secondary organic aerosol (SOA), sea salt and mineral dust, are represented by three lognormal size modes (i.e., Aitken, accumulation and coarse modes) of the modal aerosol module (MAM3) (Liu et al., 2012). The detailed aerosol representation in CAM5 was provided in Liu et al. (2012) and Wang et al. (2013). The aerosol mixing states consider both internal (within a same mode) and external mixing (between modes). On top of the default CAM5, additional modifications that improve the representation of aerosol wet scavenging and convective transport (Wang et al., 2013) are also included in the model version used for this study.

In this study, simulations were conducted with a horizontal resolution of $1.9° \times 2.5°$ and 30 vertical layers up to 3.6 hPa in the year 2020. The anthropogenic emissions used in the baseline simulation are derived from the MEIC (Multi-resolution Emission Inventory of China) inventory (Zheng et al., 2018), referred to here as the baseline experiment, while emissions for the other countries use the SSP (Shared Socioeconomic Pathways) 2–4.5 scenario data set under CMIP6 (the Coupled Model Intercomparison Project Phase 6). Emissions in year 2017 are used as the baseline during the simulation period considering the time limit of MEIC inventory. To better estimate the impact of restricted human activities

on emission reductions owing to the COVID-19 lockdown (referred to as the Covid experiment), we updated China's emission inventory from January to March 2020 based on the provincial total emission reduction ratio in Huang et al. (2020). Emissions from the transportation sector are decreased by 70 %. The remaining emission reduction, by excluding transport reduction from the total emission reduction, are evenly distributed to other sectors, including industry, power plants, residential, international shipping and waste treatment from January to March 2020 compared to the baseline emission in 2017. Unless otherwise specified, all the results in this study are derived from the Covid experiment.

The sea surface temperature, sea ice concentrations, solar radiation and greenhouse gas concentrations are fixed at present-day climatological levels. To capture the large-scale atmospheric circulations during COVID-19, we nudge the model wind fields toward the MERRA-2 (Modern-Era Retrospective Analysis for Research and Applications, version 2) reanalysis (Gelaro et al., 2017) from April 2019 to March 2020 repeatedly for 6 years. Only model results from the last year are used to represent year 2020, with the first 5 years as model spin-up. In this study, we analyze the transport pathways and source attribution of aerosols during the 3 weeks that had the largest number of newly diagnosed COVID-19 cases (Fig. S1 in the Supplement, hereafter referred to as "week 1", 30 January–5 February; "week 2", 6 February–12 February, and "week 3", 13 February–19 February), when unexpected hazardous air pollution events also occurred during this time period (Huang et al., 2020; Le et al., 2020).

2.2 Explicit aerosol source tagging and source regions

To examine the source apportionment of aerosols in China, the Explicit Aerosol Source Tagging (EAST) technique was implemented in CAM5, which has been utilized in many aerosol source attribution studies (e.g., Wang et al., 2014; Yang et al., 2017a, b, 2018a, b, c, 2019b, 2020; Ren et al., 2020). Different from the emission sensitivity method that assumes a linear response to emission perturbation and the traditional backward trajectory method, aerosols from each tagged region or sector are calculated independently in EAST within one single simulation. Without relying on a set of model simulations with emission perturbations or assuming constant decaying rate, EAST is more accurate and time saving than the source apportionment method mentioned above. In addition to the sulfate, BC and POM species that were tagged in previous studies (e.g., Yang et al., 2020), SOA and precursor gas are now also tagged in the EAST. These types of aerosols from independent source regions and sectors can be explicitly tagged and tracked simultaneously. In this study, focusing on the aerosols in China during the COVID-19 outbreak period, the domestic aerosol and precursor emissions from eight geographical source regions (Fig. 1), northeastern China (NEC), the North China Plain (NCP), eastern China (ESC), southern China (STC), central western China (CWC), southwestern China (SWC), northwestern China (NWC), the Himalayas and Tibetan Plateau (HTP), and the rest of the world (ROW), are tagged separately.

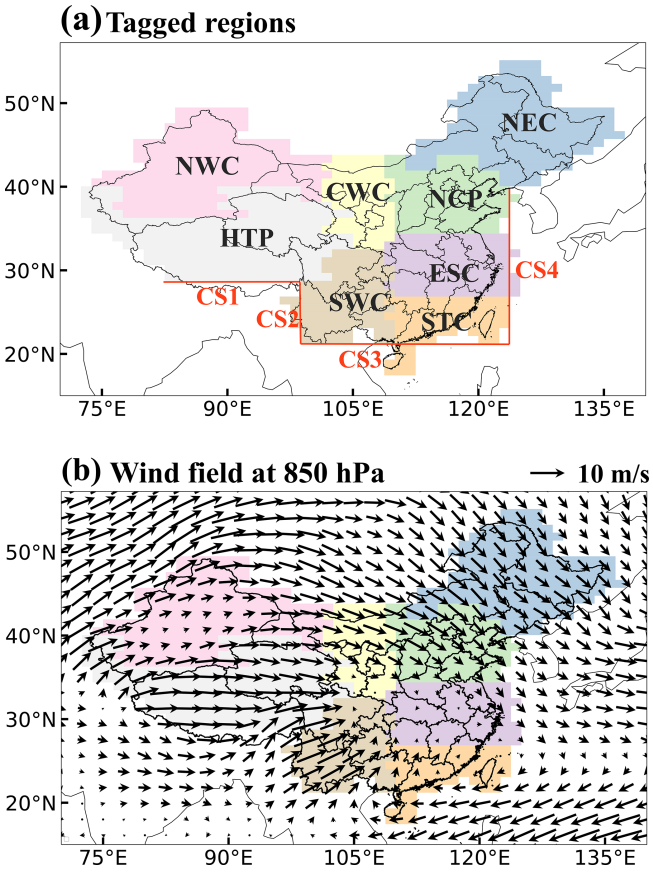

Figure 1. **(a)** Tagged source regions (NEC: northeastern China; NCP: North China Plain; ESC: eastern China; STC: southern China; CWC: central western China; SWC: southwestern China; NWC: northwestern China; HTP: Himalayas and Tibetan Plateau; ROW: rest of the world) and **(b)** mean wind field (units: $\mathrm{m\,s^{-1}}$, vectors) at 850 hPa during the 3 weeks of the study from 30 January to 19 February, which had the largest number of newly diagnosed COVID-19 cases. Lines in **(a)** mark the cross sections (CS) defined to study the transport of aerosols to and from China.

3 Model evaluation

Many previous studies have assessed the spatial distribution and seasonal to decadal variations in aerosol concentrations in China and worldwide simulated by CAM5 with the observations (e.g., Wang et al., 2013; Yang et al., 2017a, b, 2018b, c, 2020). In order to evaluate the model's performance when simulating aerosols during the COVID-19 outbreak period in China, the surface concentrations of $PM_{2.5}$, estimated as the sum of sulfate, BC, POM and SOA for model results, during the analyzed time periods are compared with mea-

surements from the China National Environmental Monitoring Center (CNEMC), as shown in Fig. 2a. The model reasonably reproduces the overall spatial distribution of near-surface $PM_{2.5}$ concentrations during the three time periods, with high values over the North China Plain and low values in western China. However, as reported in many CAM5 model studies (e.g., Yang et al., 2017a, b), the model underestimates the $PM_{2.5}$ concentrations with normalized mean biases (NMBs) of $-55\,\% \sim -49\,\%$ compared to the available site observations (Fig. S2). The discrepancies are related to coarse-resolution model sampling bias relative to the observational sites, uncertainties in aerosol emissions, wet removal and gas–particle exchange. In addition, the model version used in this study is not able to simulate nitrate and ammonium aerosols, which are also the main components of $PM_{2.5}$ (Kong et al., 2020; Xu et al., 2019).

The long-distance transport of aerosols mainly occurs in the upper troposphere rather than near the surface (Hadley et al., 2007; Zhang et al., 2015). Aerosols are lifted from the atmospheric boundary layer of the emission source regions to the free troposphere and then undergo the transboundary and intercontinental transport effectively driven by the upper tropospheric circulations. Therefore, it is helpful to analyze the relative contributions of local and nonlocal sources by focusing on the column burden of aerosols. Figure 2b presents spatial distributions of simulated mean column burden of $PM_{2.5}$ during the three time periods (week 1, 30 January–5 February; week 2, 6–12 February; and week 3, 13–19 February) that had the largest number of newly diagnosed COVID-19 cases. The contrast in column burden does not differ significantly from that of near-surface concentrations. Compared to week 3, week 1 and week 2 have higher $PM_{2.5}$ loading, with values in the range of 20–40 and 20–30 $\mathrm{mg\,m^{-2}}$, respectively, over the North China Plain and in eastern China and southern China, while the $PM_{2.5}$ loading in week 3 is relatively low compared to week 1 and week 2, with values mostly ranging from 10 to 20 $\mathrm{mg\,m^{-2}}$. Note that the column burden of $PM_{2.5}$ in South Asia and Southeast Asia is higher than 20 $\mathrm{mg\,m^{-2}}$ in the three time periods and reaches up to 50 $\mathrm{mg\,m^{-2}}$ in week 2, which potentially influences aerosol concentrations in China through transboundary transport.

4 Transport pathways

The explicit aerosol tagging technique can clearly identify the transport pathways of aerosols moving from their source regions to their destination. Figure 3 shows the spatial distribution of mean column burden of simulated $PM_{2.5}$ originating from the six tagged source regions in central and eastern China and outside of China during the three time periods. Aerosols and/or precursor gases emitted from the various regions follow quite different transport pathways determined by their source locations, meteorological conditions, emission injection height, and the physical and chemical characteristics of aerosol species. Aerosols from northeastern China are transported southeastward by the northwesterly winds (Fig. 1b). From the North China Plain, aerosols can be transported either southward reaching eastern, southern and southwestern China during week 1 or across eastern coast of China to the oceanic region during weeks 2–3. Aerosols originating from eastern China move straight to southwestern and southern China during weeks 1–2, while they also entered the North China Plain during weeks 2–3. Aerosols emitted from southern China and central western China have no obvious transport due to their relatively weak emissions. In addition to the local impact, emissions from southwestern China mostly affect southern China and eastern China. Air parcels with high levels of $PM_{2.5}$ from South Asia and Southeast Asia moved into southwestern, southern, and eastern China and even the North China Plain during the three time periods.

The vertical distributions of $PM_{2.5}$ emitted from the six major tagged source regions are shown in Figs. S3 and S4. $PM_{2.5}$ has much higher concentrations in the lower troposphere and decreases with increasing height. During weeks 1–2, owing to the presence of high $PM_{2.5}$ loadings, a stronger vertical mixing and transport brought more $PM_{2.5}$ to the upper troposphere compared to that during Week 3. High concentrations of $PM_{2.5}$ originating from the North China Plain extended southeastward by strong northwesterly winds. Weak winds over eastern China led to accumulations of $PM_{2.5}$ within this region, which is consistent with the findings in Yang et al. (2017a). Strong southwesterly winds in the south of southwestern China and weak winds in the north of this region produced convergences and updrafts that lifted aerosols up to 700 hPa.

Considering that emissions outside China contribute greatly to $PM_{2.5}$ concentrations in southwestern China through transboundary transport (Yang et al., 2017a) and that aerosols from East Asia can be transported to the North Pacific and even North America (Yu et al., 2008; Yang et al., 2018c), it is of great importance to study the inflow and outflow of $PM_{2.5}$ across the boundaries of China. Figures 4 and 5 show the vertical distribution of $PM_{2.5}$ concentrations resulting from emissions within and outside China over 29° N, 88° E and 21° N around the south boundaries (cross sections (CSs) 1–3 in Fig. 1a) and 123° N around the east boundary (CS 4 in Fig. 1a) of mainland China. Over the southern border, $PM_{2.5}$ concentrations are more influenced by transboundary transport of aerosols from the ROW than those originating from domestic emissions. The high concentrations of $PM_{2.5}$ from South Asia and Southeast Asia are lifted into the free atmosphere of the Tibetan Plateau and Yunnan-Guizhou Plateau and then transported to southern and southwestern China by southwesterly winds. Over the North China Plain and eastern China, northwesterly winds at 35–45° N and southwesterly winds at 25–35° N cause aerosols to accumulate in the lower atmosphere and then export across the eastern border of China below 700 hPa.

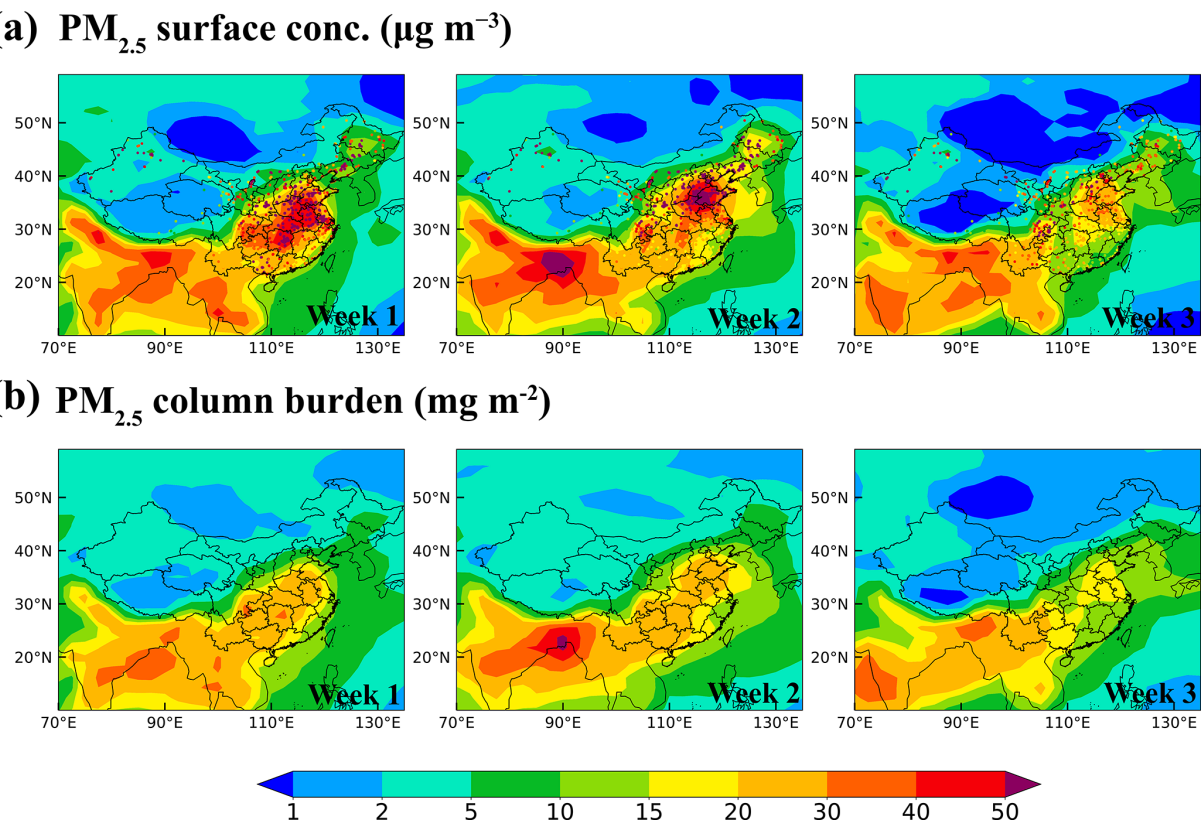

Figure 2. Spatial distribution of **(a)** the simulated and observed mean near-surface $PM_{2.5}$ concentrations ($\mu g\,m^{-3}$) and **(b)** $PM_{2.5}$ column burden ($mg\,m^{-2}$) during 30 January–5 February (week 1), 6–12 February (week 2) and 13–19 February (week 3).

5 Source apportionment of $PM_{2.5}$ in China during the COVID-19 outbreak

5.1 Source contributions to $PM_{2.5}$ burden

Figure 6 shows the simulated relative contributions in percentage to $PM_{2.5}$ column burden from local-source emissions, regional transport from the untagged regions of China (rest of China, RCN) and rest of the world (ROW). Over the North China Plain, where emissions are relatively high, $PM_{2.5}$ column burden is dominated by local emissions during the three time periods. In contrast, regions with relative low emissions are mainly affected by nonlocal sources, especially by foreign contributions. Emissions from the ROW contribute a large amount to $PM_{2.5}$ burden over northeastern, southern, central western, southwestern, and northwestern China and the Tibetan Plateau. $PM_{2.5}$ burden in eastern China is greatly contributed by the sources from RCN, especially in Week 1 when regional transport of $PM_{2.5}$ from the North China Plain is relatively strong (Fig. S4).

Table 1 summarizes the contributions of tagged source regions to the $PM_{2.5}$ burden over different receptor regions in China. In northeastern China, 36 %–43 % of the $PM_{2.5}$ column burden comes from local emissions, while a larger portion (39 %–54 %) is contributed by emissions from the ROW during the three time periods. The impacts of nonlocal sources within China on $PM_{2.5}$ burden are relatively low in northeastern China during week 1, with a contribution of less than 5 %, while RCN is responsible for 23 % and 25 % during week 2 and week 3, respectively.

Over the North China Plain, the majority of the $PM_{2.5}$ burden is attributed to local emissions in all cases, with local contributions ranging from 40 % to 66 %. Emissions from the North China Plain also produce a widespread impact on $PM_{2.5}$ over neighboring regions. The sources from the North China Plain account for 14 %–33 % of the $PM_{2.5}$ burden in eastern China and 7 %–23% in southern China during the three time periods.

In eastern China, local emissions account for 27 %–40 % of $PM_{2.5}$ column burden, while the ROW contributes 20 %–45 %. Southern China and central western China have 13 %–18 % and 25 %–31 % of local-source contributions, respectively, whereas 37 %–64 % are due to emissions from outside China in these two regions. In southwestern China, 15 %–18 % of the $PM_{2.5}$ burden originates from local emissions and 7 %–24 % is from RCN. ROW emissions play important roles in affecting $PM_{2.5}$ burden over this region, with relative contributions in a range of 59 %–78 % during the three time periods, which is associated with the transboundary transport

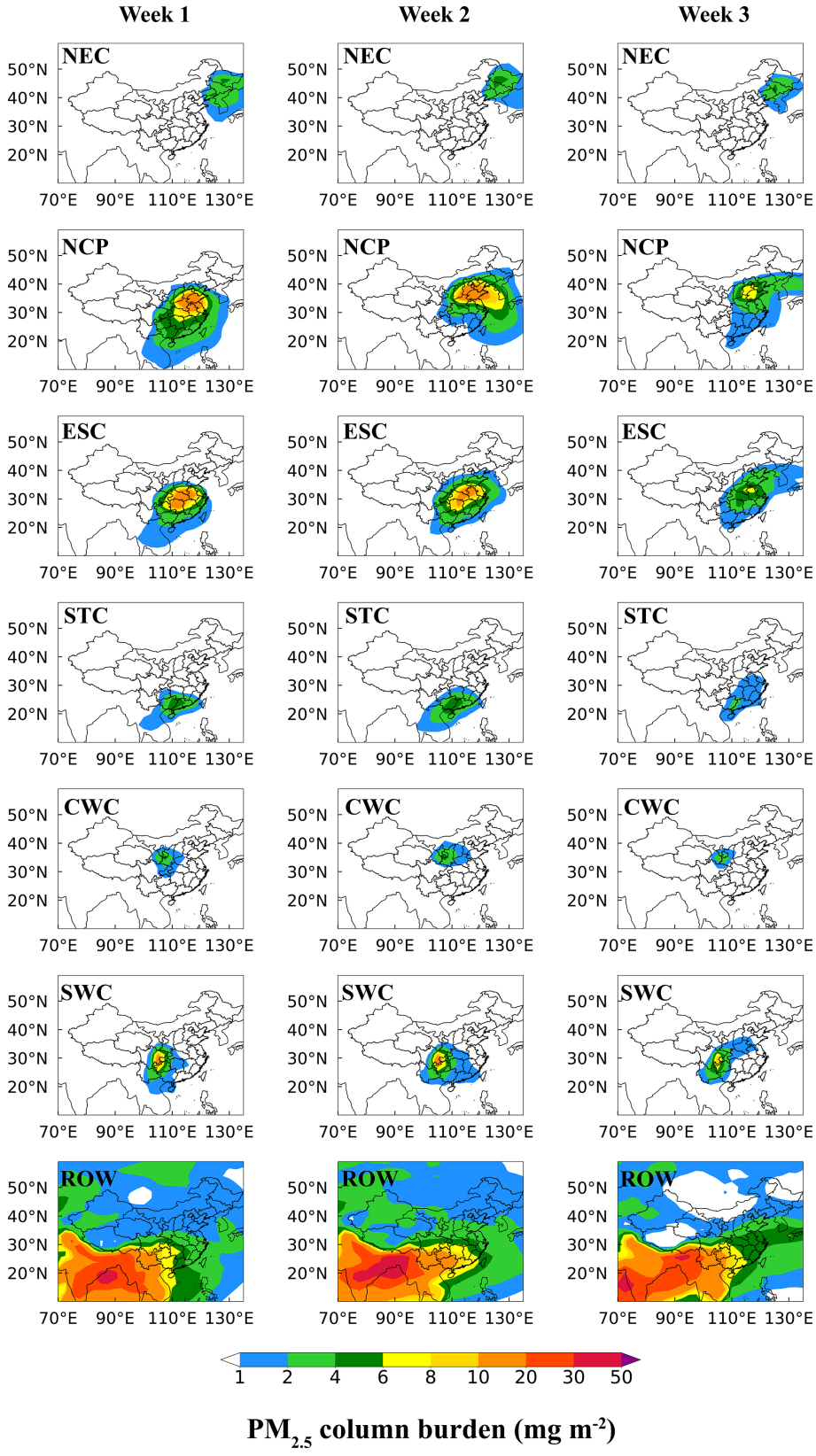

Figure 3. Spatial distribution of $PM_{2.5}$ column burden (mg m^{-2}) originating from the six major source regions in China (NEC, NCP, ESC, STC, CWC and SWC) and sources outside China (ROW) during the three time periods.

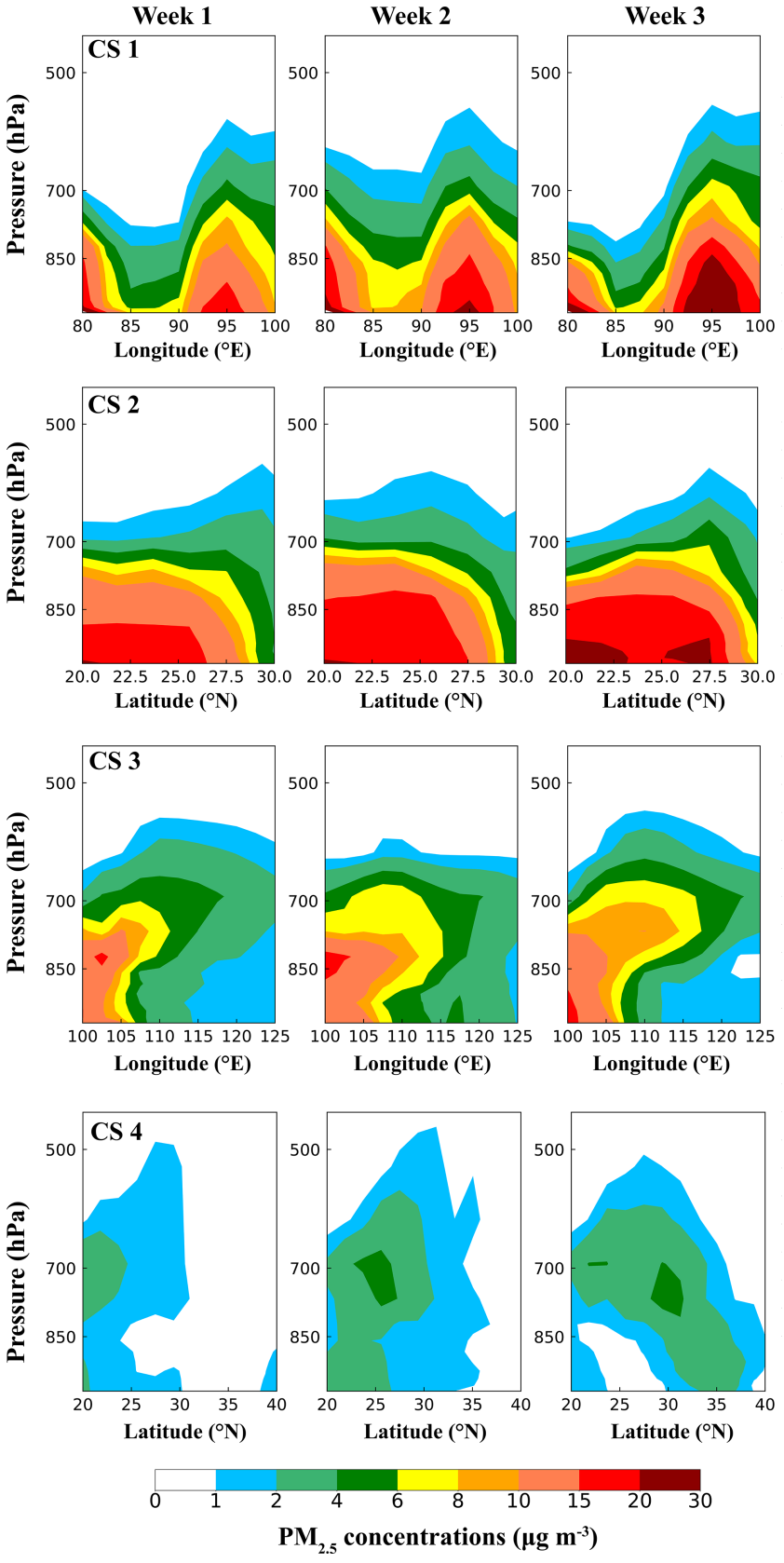

Figure 4. Vertical distributions of $PM_{2.5}$ concentrations ($\mu g\,m^{-3}$) originating from emissions outside China (i.e., ROW sources) across the latitudinal and/or longitudinal extents marked in Fig. 1, respectively, during the three time periods.

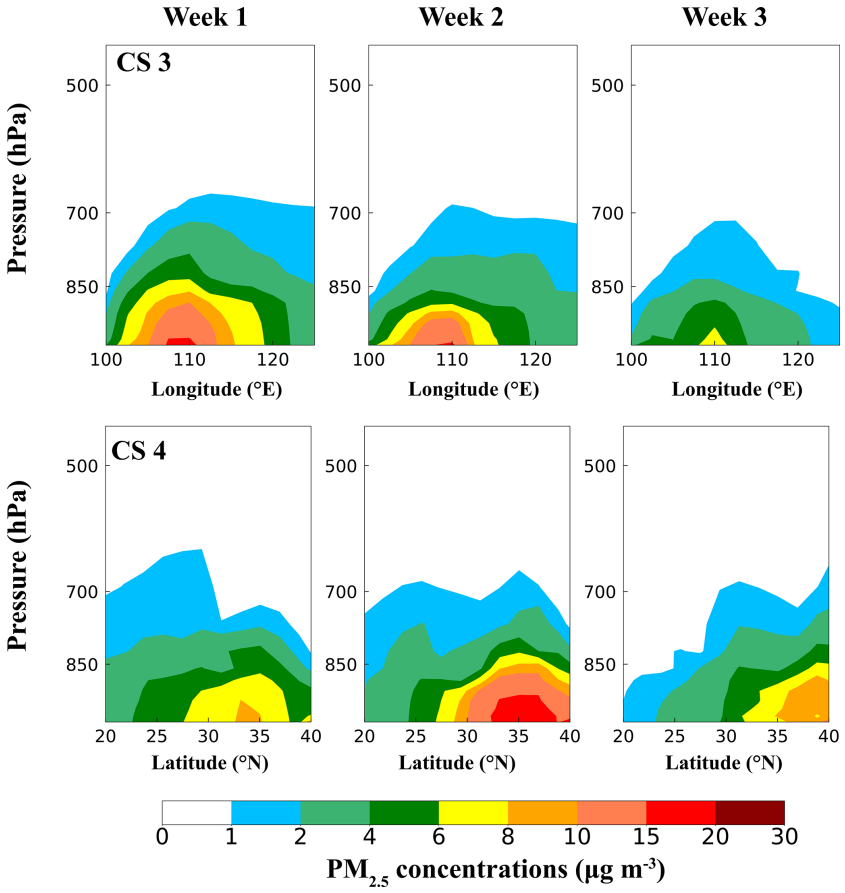

Figure 5. Vertical distributions of $PM_{2.5}$ concentrations ($\mu g\,m^{-3}$) originating from domestic emissions in China across the latitudinal and/or longitudinal extents marked in Fig. 1, respectively, during the three time periods. The values along CS 1 and CS 2 are negligibly small.

by southwesterly winds. $PM_{2.5}$ burden over northwestern China and the Himalayas and Tibetan Plateau, where there are relatively low local emissions, is strongly influenced by nonlocal sources, and more than 70 % of the $PM_{2.5}$ burden originates from emissions outside China.

5.2 Aerosol source attribution during polluted days

In spite of the large reductions in emissions, severe air pollution events still occurred in China during the COVID-19 lockdown. Source attribution of $PM_{2.5}$ during polluted days in China has policy implications for future air pollution control. In Beijing, the capital of China, located on the North China Plain, a serious haze event happened from 11 to 13 February 2020 during the COVID-19 outbreak period according to observations released by CNEMC. CAM5-EAST reproduced the polluted day on 11 February over the North China Plain. In this study, the most polluted day is defined as the day with the highest daily $PM_{2.5}$ concentration in February 2020 for each receptor region in China. Figure 7 presents the composite differences in near-surface $PM_{2.5}$ concentrations and 850 hPa wind fields between the most polluted day and normal days (all days in February 2020) for each receptor region. The local- and nonlocal-source contributions to the $PM_{2.5}$ differences are summarized in Fig. 8.

Unexpectedly, near-surface $PM_{2.5}$ concentrations over the North China Plain and in eastern China experienced remarkable increases during the most polluted day of COVID-19 lockdown. The simulated $PM_{2.5}$ concentrations increased, with the largest increases being a more than $20\,\mu g\,m^{-3}$ over the North China Plain and in eastern China; a $10\,\mu g\,m^{-3}$ maximum increase in southwestern China; and a $5\,\mu g\,m^{-3}$ increase in northeastern, southern, and central western China during the most polluted days compared to the normal days.

The increase in near-surface $PM_{2.5}$ concentrations during the most polluted day over northeastern China is largely influenced by the local emissions, which contribute to a regional averaged concentration increase of $1.1\,\mu g\,m^{-3}$. This is mainly due to the accumulation of local aerosols under the weakened prevailing northwesterly winds over this region.

When the $PM_{2.5}$ pollution occurred over the North China Plain on 11 February 2020, which was also reported as the polluted day in observations (Huang et al., 2020), the concentration of $PM_{2.5}$ was $16.1\,\mu g\,m^{-3}$ higher than that of normal days. The contribution from local emissions accounts

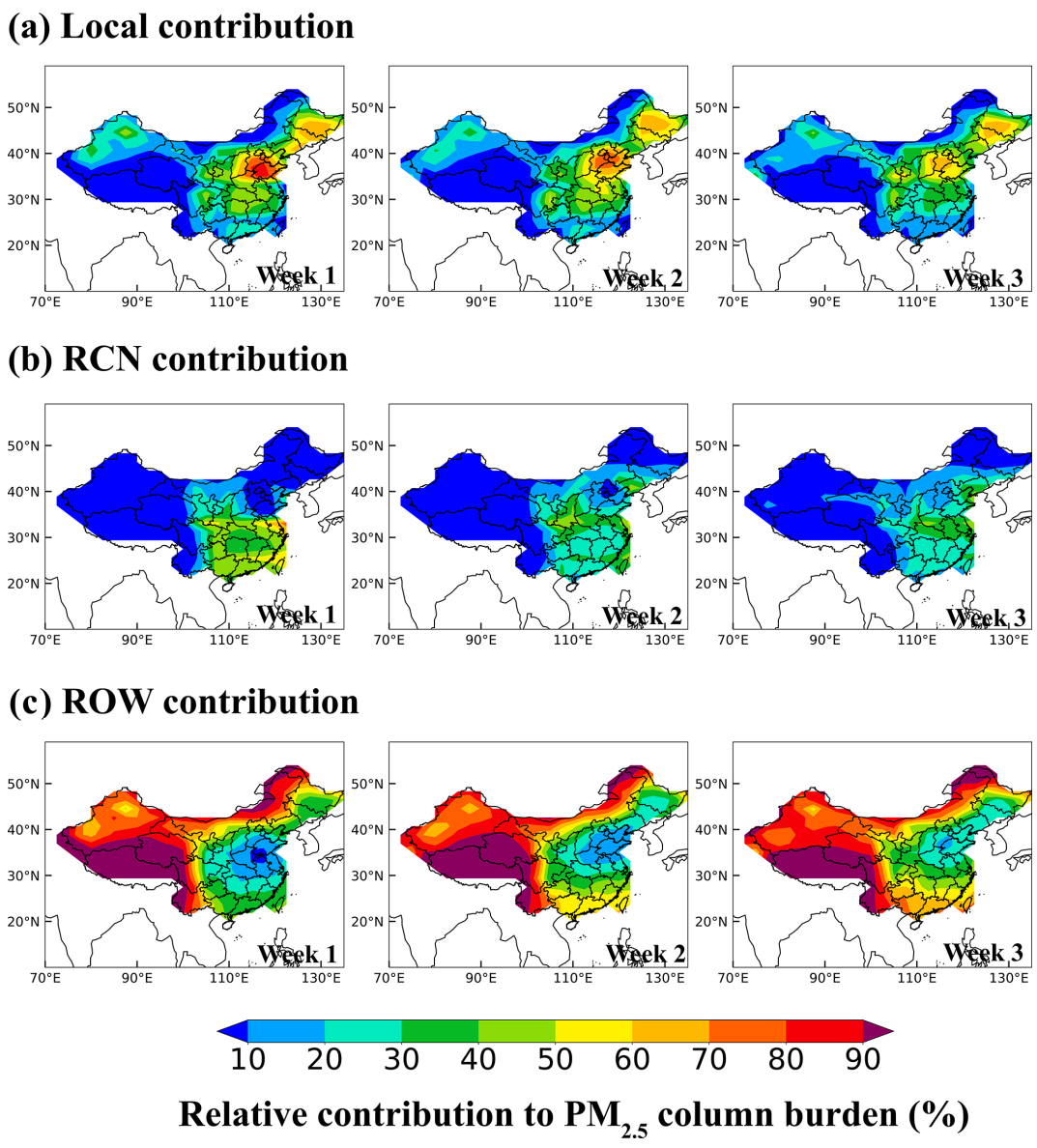

Figure 6. Relative contributions (%) of **(a)** local emissions, **(b)** the emissions from the rest of China (RCN) and **(c)** all sources outside China (rest of the world, ROW) to $PM_{2.5}$ column burden during the three time periods.

for 66 % of the averaged increase, which was related to the stagnant air condition (i.e., weakened lower tropospheric winds) resulting from the anomalous mid-tropospheric high-pressure system located at the climatological location of the East Asia trough (Fig. S5). Sources from eastern China also explain 4.3 $\mu g\,m^{-3}$ (27 %) of the total increase over the North China Plain.

During the most polluted day in eastern China (the same day as the most polluted day over North China Plain), the concentration of $PM_{2.5}$ was 16 $\mu g\,m^{-3}$ higher than that of normal days, which is primarily contributed by the local emissions. While the contribution from the North China Plain decreased on the most polluted day, the anomalous southerly winds brought more aerosols from southern China and the ROW into eastern China, contributing to 4 % and 10 % aerosol increase, respectively.

Owing to the enhanced northerly winds during the most polluted days, emissions from the North China Plain and eastern China contribute 33 % and 39 % of the increase in $PM_{2.5}$ concentration over Southern China, respectively. The most polluted day in central western China is mostly caused by local emissions (65 % of the total increase).

When southwestern China was under polluted conditions, $PM_{2.5}$ concentration increased by 2.1 $\mu g\,m^{-3}$. Emissions from the ROW, especially those from South Asia and Southeast Asia, are of great significance to the increase in $PM_{2.5}$

Table 1. Fractional contributions of emissions from nine tagged source regions (vertical axis) to mean $PM_{2.5}$ column burden in eight receptor regions (horizontal axis) during the three time periods (week 1, 30 January–5 February; week 2, 6–12 February; and week 3, 13–19 February).

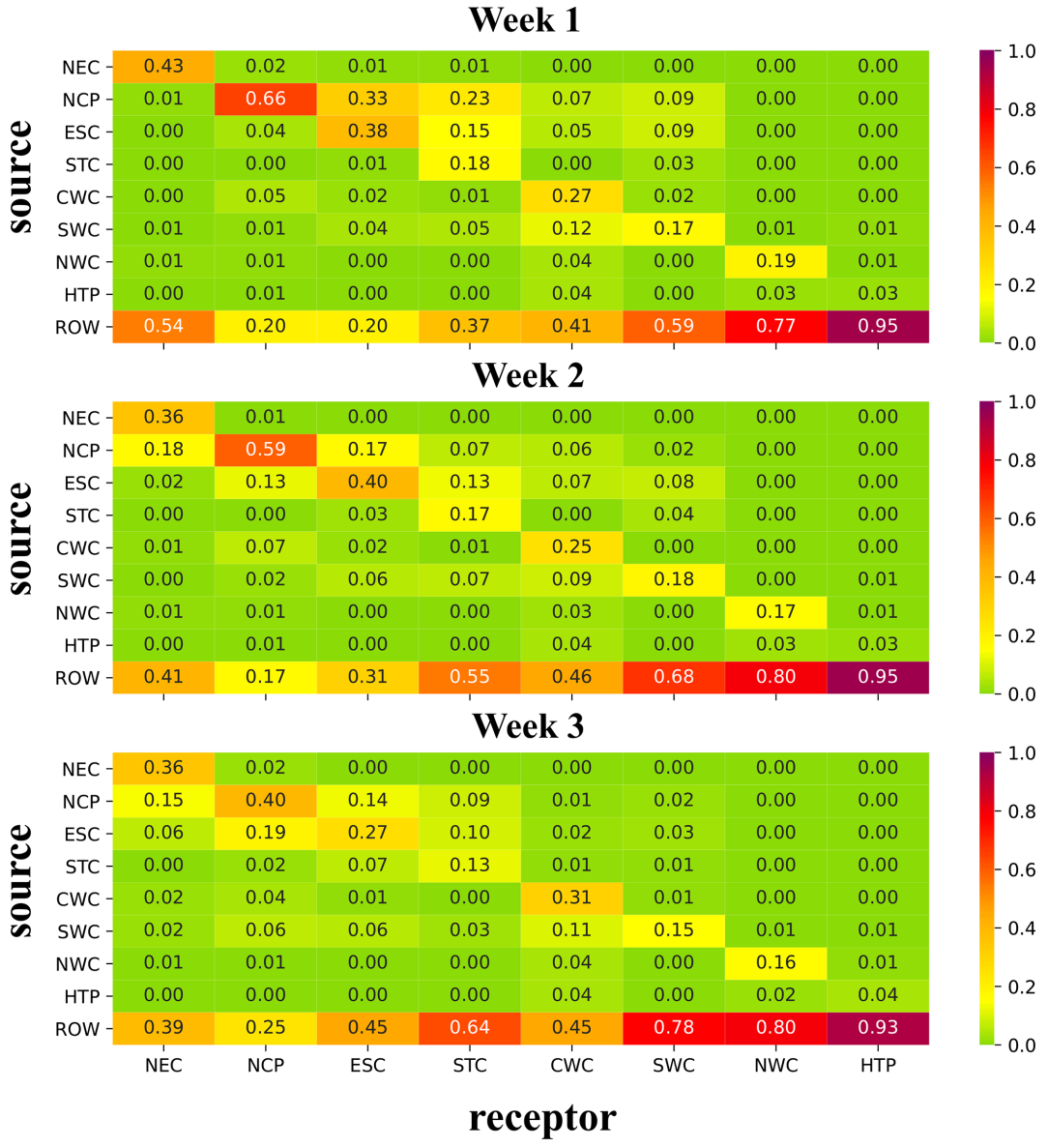

concentrations due to the enhanced southwesterly winds over this region. The relative contribution from ROW emissions is more than 50 % over southwestern China during the most polluted day. This highlights that the important role of transboundary transport needs to be considered when controlling local emissions to improve air quality in the near future.

6 Conclusion and discussions

The COVID-19 pandemic disrupted human activities and led to abrupt reductions in anthropogenic emissions. This study first investigated the source contributions to $PM_{2.5}$ over various regions covering all of China during the COVID-19 pandemic. We pay attention to not only local emissions but also to the impacts from regional and foreign transport of aerosols. An explicit aerosol source tagging is implemented in the Community Atmosphere Model version 5 (CAM5-EAST) to examine the aerosol transport pathways and source attribution of $PM_{2.5}$ in China during the first few weeks of the COVID-19 outbreak (week 1, 30 January–5 February; week 2, 6–12 February; and week 3, 13–19 February). The contributions of emissions to $PM_{2.5}$ originating from eight source regions in mainland China, i.e., northeastern China, the North China Plain, eastern China, southern China, central western China, southwestern China, northwestern China, and the Himalayas and Tibetan Plateau, and sources outside

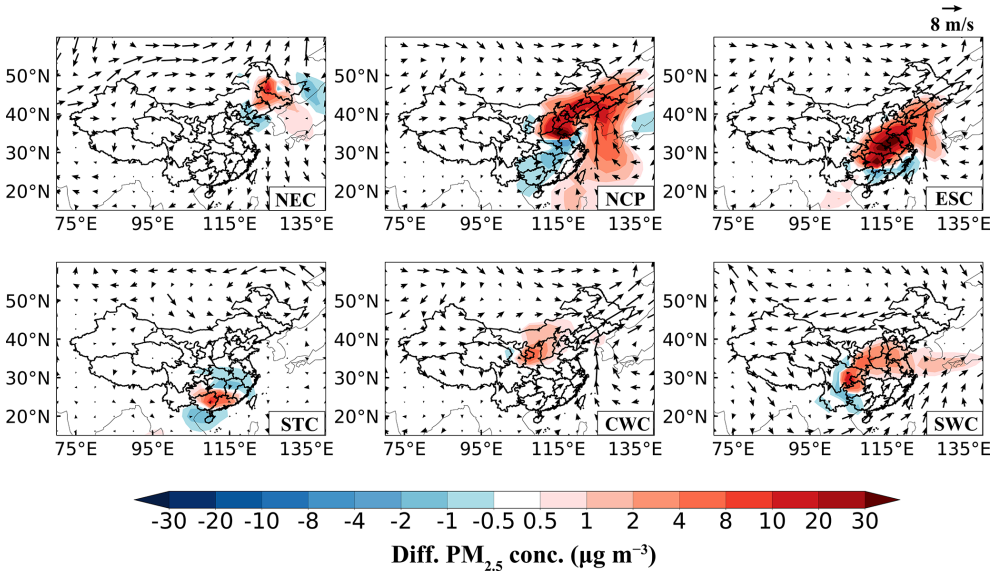

Figure 7. Composite differences in winds at 850 hPa ($m\,s^{-1}$) and near-surface $PM_{2.5}$ concentrations (μm^{-3}) between the most polluted and normal days in February 2020. The most polluted day is defined as the day with the highest daily $PM_{2.5}$ concentration in February 2020 in each receptor region in China.

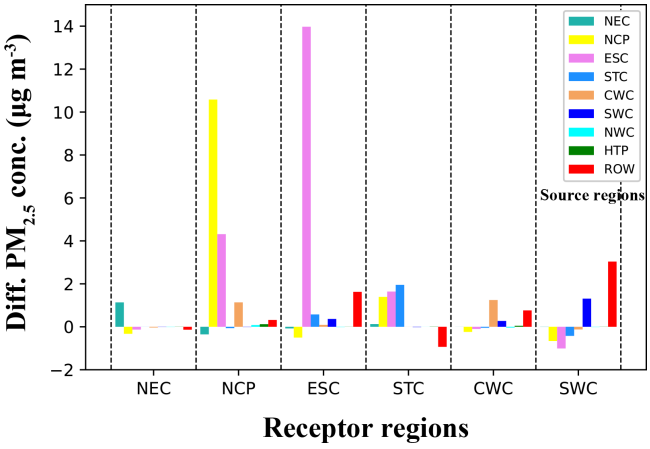

Figure 8. Composite differences in near-surface $PM_{2.5}$ concentrations (μm^{-3}) averaged over receptor regions (marked on the horizontal axis) in China between the most polluted and normal days in February 2020 originating from individual source regions (corresponding color bars in each column).

China (ROW) to near-surface concentrations, column burdens, transport pathways of $PM_{2.5}$ and haze formation in different receptor regions in China are quantified in this study.

Aerosols emitted from the North China Plain, where the air quality is often poor, was transported through eastern China and reach southwestern China during the three time periods. Similarly, aerosols from eastern China moved straight to southern China and Southwestern China during week 1 and week 2, and a significant portion also entered the North China Plain during week 2 and week 3.

Across the southern boundary of mainland China, high concentrations of $PM_{2.5}$ from South Asia and Southeast Asia are lifted into the free atmosphere and then transported to southern and southwestern China. In addition, $PM_{2.5}$ from the North China Plain and eastern China can also be brought out of China via westerly winds, mostly below 700 hPa.

$PM_{2.5}$ in China is affected by not only local emissions but also long-range transport of pollutants from distant source regions. Over the North China Plain, 40 %–66 % of the $PM_{2.5}$ burden is attributed to local emissions during the COVID-19 outbreak. They also impact $PM_{2.5}$ in neighboring regions, accounting for 14 %–33 % of the $PM_{2.5}$ burden in eastern China and 7 %–23 % in southern China during the three time periods. Northeastern China has 36 %–43 % local-source contributions to its $PM_{2.5}$ column burden, while 39 %–54 % is contributed by emissions from the ROW during the three time periods. In eastern China, local emissions explain 27 %–40 % of the $PM_{2.5}$ burden, while the ROW contributes 20 %–45 %. In southwestern China, 59 %–78 % of the $PM_{2.5}$ burden is contributed by emissions from the ROW. Over northwestern China and the Himalayas and Tibetan Plateau, ROW emissions have a great contribution of more than 70 % to the $PM_{2.5}$ column burden.

In this study, the most polluted day is defined as the day with the highest daily $PM_{2.5}$ concentration in February 2020 for each receptor region in China. The transport from outside of China only has a great impact on some specific regions in China. In southwestern China, the relative contribution from ROW emissions, especially those from South Asia and Southeast Asia, to the increment of $PM_{2.5}$ concentration during the most polluted days compared with normal days is

more than 50 %. It is consistent with previous studies where emissions from South Asia and Southeast Asia have an important impact on air quality in southwestern China (Yang et al., 2017a; Zhu et al., 2016, 2017). For other receptor regions in China (northeastern China, the North China Plain, eastern China, southern China and central western China), $PM_{2.5}$ concentrations are largely contributed by local emissions during the most polluted days compared with normal days. In the future with emissions reductions for better air quality in China, decreasing air pollution should consider aerosols from both Chinese local emissions and pollutant transport from outside of China.

Despite the large reductions in emissions, near-surface $PM_{2.5}$ concentrations over the North China Plain and in eastern China increased a lot during the most polluted days of the COVID-19 lockdown (with the highest daily $PM_{2.5}$ concentration in February 2020), with the largest increases of more than 20 $\mu g\,m^{-3}$. In addition to local emissions, regional transport of pollutants is also an important factor that causes haze events in China. The increases in $PM_{2.5}$ concentrations during the most polluted days over the North China Plain and eastern China are largely influenced by the stagnant air conditions resulting from the anomalous high-pressure system and weakening of winds, which led to reduced ventilation and aerosol accumulation over the North China Plain, together with an increase in aerosol inflow from regional transport. During the most polluted day in southwestern China, ROW contributed over 50 % of the $PM_{2.5}$ concentration increase, with enhanced southwesterly winds that drive pollution transport from South Asia and Southeast Asia. This indicates that regional transport and unfavorable meteorology need to be taken into consideration when controlling local emissions to improve air quality in the near future.

To highlight the roles of regional and foreign transport, the differences between the Covid and baseline simulations in relative contributions to $PM_{2.5}$ burden from local, regional (RCN) and foreign (ROW) emissions are given in Fig. S6. During the COVID-19 period, the local and RCN emission contributions to $PM_{2.5}$ were 1 %–4 % lower than those in baseline experiment over the North China Plain and northeastern China. In eastern China, the contribution from the local emissions decreased by 3 %–4 % compared with the baseline experiment, while the contribution from the ROW increased by more than 5 %. In southern China, 50 %–70% of the $PM_{2.5}$ burden is contributed by emissions from the ROW in the baseline experiment. During the COVID-19 period with low emission levels, the contribution from ROW to $PM_{2.5}$ burden in southern China had an increase of more than 5 %. This indicates that the important role of transboundary transport needs to be considered when controlling local emissions to improve air quality in the near future.

Many studies have examined the importance of meteorology in regional air quality during the COVID-19 lockdown period and emphasized that when meteorology is unfavorable, abrupt emissions reductions cannot avoid severe air pollution (Le et al., 2020; Sulaymon et al., 2021; Shen et al., 2021). Through model simulations, Le et al. (2020) found that abnormally high humidity promotes the heterogeneous chemistry of aerosols, which contributed to the increase in $PM_{2.5}$ by 12 % in northern China during the city lockdown period. Sulaymon et al. (2021) found a significant increase in $PM_{2.5}$ concentrations caused by unfavorable meteorological conditions in the Beijing–Tianjin–Hebei region during the lockdown period based on Community Multiscale Air Quality (CMAQ) model simulations. By analyzing the observational data and model simulations, Shen et al. (2021) reported that 50 % of the pollution episodes during the COVID-19 lockdown in Hubei were due to the stagnant meteorological conditions. Huang et al. (2020) found that the stagnant air conditions and enhanced atmospheric oxidizing capacity caused a severe haze event during the same time period. In line with previous studies, we also revealed the stagnant air conditions under the anomalous high-pressure system during the most polluted day over the North China Plain. In addition to the meteorological conditions, the effect of foreign transport was also raised in this study as causing aerosol pollution in southwestern China during COVID-19 outbreak.

There are a few uncertainties in this study. The CAM5 model has low biases when reproducing the near-surface $PM_{2.5}$ concentrations in China compared to observations, in part due to its incapability of simulating some aerosol components of $PM_{2.5}$ (e.g., ammonium and nitrate), excessive aerosol wet removal during long-range transport (Wang et al., 2013) and uncertainties in observations. In the majority of the climate models, the simulation of nitrate and ammonium aerosols is not included in the aerosol schemes, partly due to the complexity of calculation efficiency. For example, of the many CMIP6 models, only two of them provide nitrate and ammonium mass mixing ratios. Many previous studies have evaluated the global climate model performance in reproducing aerosol concentrations (e.g., Fan et al., 2018; Shindell et al., 2013; Yang et al., 2017a, b). In general, the models can simulate aerosols in North America and Europe well but significantly underestimate aerosols in East Asia by about −36 % to −58 % compared with observations. This can lead to an underestimation of aerosols contributed by Chinese local emissions in magnitudes but might not change the main conclusions of this study. Uncertainties in the estimate of emission reductions in different source regions during the COVID-19 pandemic can also introduce uncertainties to our results. During the COVID-19 lockdown, greenhouse gas emissions also decreased (Le Quéré et al., 2020), but the effect of greenhouse gas reduction on meteorology that potentially influences aerosol distributions was not taken into consideration. Nevertheless, this study is the first attempt to provide source apportionment of aerosols covering all of China during the COVID-19 outbreak, which is beneficial to the investigation of policy implications for future air pollution control.

Code and data availability. The CAM5 model is available at http://www.cesm.ucar.edu/models/cesm1.2/ (UCAR, 2021). The CAM5-EAST model code and results can be made available upon request. The surface $PM_{2.5}$ observations are from the China National Environmental Monitoring Center (CNEMC, https://doi.org/10.5281/zenodo.5564726, Yang, 2021).

Supplement. The supplement related to this article is available online at: https://doi.org/10.5194/acp-21-15431-2021-supplement.

Author contributions. YY and LR designed the research. YY performed the model simulations. LR analyzed the data. All authors discussed the results and wrote the paper.

Competing interests. The contact author has declared that neither they nor their co-authors have any competing interests.

Disclaimer. Publisher's note: Copernicus Publications remains neutral with regard to jurisdictional claims in published maps and institutional affiliations.

Acknowledgements. Hailong Wang acknowledges support from the U.S. Department of Energy (DOE), Office of Science, Office of Biological and Environmental Research (BER). The Pacific Northwest National Laboratory (PNNL) is operated for DOE by the Battelle Memorial Institute under contract no. DE-AC05-76RLO1830.

Financial support. This research has been supported by the National Key Research and Development Program of China (grant nos. 2020YFA0607803 and 2019YFA0606800) and the National Natural Science Foundation of China (grant no. 41975159).

Review statement. This paper was edited by Kostas Tsigaridis and reviewed by two anonymous referees.

References

Anderson, T. L., Charlson, R. J., Schwartz, S. E., Knutti, R., Boucher, O., Rodhe, H., and Heintzenberg, J.: Climate forcing by aerosol – a hazy picture, Science, 300, 1103–1104, https://doi.org/10.1126/science.1084777, 2003.

Bao, R. and Zhang, A.: Does lockdown reduce air pollution? Evidence from 44 cities in northern China, Sci. Total Environ., 731, 139052, https://doi.org/10.1016/j.scitotenv.2020.139052, 2020.

Chai, F., Gao, J., Chen, Z., Wang, S., Zhang, Y., Zhang, J., Zhang, H., Yun, Y., and Ren, C.: Spatial and temporal variation of particulate matter and gaseous pollutants in 26 cities in China, J. Environ. Sci., 26, 75–82, https://doi.org/10.1016/S1001-0742(13)60383-6, 2014.

China State Council: Action Plan on Prevention and Control of Air Pollution, China State Council, Beijing, China, available at: http://www.gov.cn/zwgk/2013-09/12/content/textunderscore2486773.htm (last access: 27 September 2020), 2013.

Dong, E., Du, H., and Gardner, L.: An interactive web-based dashboard to track COVID-19 in real time, Lancet Infect. Dis., 20, 533–534, https://doi.org/10.1016/S1473-3099(20)30120-1, 2020.

Fan, H., Zhao, C., and Yang, Y.: A comprehensive analysis of the spatio-temporal variation of urban air pollution in China during 2014–2018, Atmos. Environ., 220, 117066, https://doi.org/10.1016/j.atmosenv.2019.117066, 2020.

Fan, T., Liu, X., Ma, P.-L., Zhang, Q., Li, Z., Jiang, Y., Zhang, F., Zhao, C., Yang, X., Wu, F., and Wang, Y.: Emission or atmospheric processes? An attempt to attribute the source of large bias of aerosols in eastern China simulated by global climate models, Atmos. Chem. Phys., 18, 1395–1417, https://doi.org/10.5194/acp-18-1395-2018, 2018.

Gelaro, R., McCarty, W., Suárez, M. J., Todling, R., Molod, A., Takacs, L., Randles, C. A., Darmenov, A., Bosilovich, M. G., Reichle, R., Wargan, K., Coy, L., Cullather, R., Draper, C., Akella, S., Buchard, V., Conaty, A., da Silva, A. M., Gu, W., Kim, G., Koster, R., Lucchesi, R., Merkova, D., Nielsen, J. E., Partyka, G., Pawson, S., Putman, W., Rienecker, M., Schubert, S. D., Sienkiewicz, M., and Zhao, B.: The Modern-Era Retrospective Analysis for Research and Applications, Version 2 (MERRA-2), J. Climate, 30, 5419–5454, https://doi.org/10.1175/JCLI-D-16-0758.1, 2017.

Hadley, O. L., Ramanathan, V., Carmichael, G. R., Tang, Y., Corrigan, C. E., Roberts, G. C., and Mauger, G. S.: Trans-Pacific transport of black carbon and fine aerosol ($D < 2.5\,\mu m$) into North America, J.-Geophys. Res., 112, D05309, https://doi.org/10.1029/2006JD007632, 2007.

Heft-Neal, S., Burney, J., Bendavid, E., and Burke, M.: Robust relationship between air quality and infant mortality in Africa, Nature, 559, 254, https://doi.org/10.1038/s41586-018-0263-3, 2018.

Huang, X., Ding, A., Gao, J., Zheng, B., Zhou, D., Qi, X., Tang, R., Ren, C., Nie, W., Chi, X., Wang, J., Xu, Z., Chen, L., Li, Y., Che, F., Pang, N., Wang, H., Tong, D., Qin, W., Cheng, W., Liu, W., Fu, Q., Chai, F., Davis, S. J., Zhang, Q., and He, K.: Enhanced secondary pollution offset reduction of primary emissions during COVID-19 lockdown in China, Natl. Sci. Rev., 8, nwaa137, https://doi.org/10.1093/nsr/nwaa137, 2020.

Hurrell, J. W., Holland, M. M., Gent, P. R., Ghan, S., Kay, J. E., Kushner, P. J., Lamarque, J. F., Large, W. G., Lawrence, D., Lindsay, K., Lipscomb, W. H., Long, M. C., Mahowald, N., Marsh, D. R., Neale, R. B., Rasch, P., Vavrus, S., Vertenstein, M., Bader, D., Collins, W. D., Hack, J. J., Kiehl, J., and Marshall, S.: The Community Earth System Model A Framework for Collaborative Research, Bull. Am. Meteorol. Soc., 94, 1339–1360, https://doi.org/10.1175/BAMS-D-12-00121.1, 2013.

Kong, L., Feng, M., Liu, Y., Zhang, Y., Zhang, C., Li, C., Qu, Y., An, J., Liu, X., Tan, Q., Cheng, N., Deng, Y., Zhai, R., and Wang, Z.: Elucidating the pollution characteristics of nitrate, sulfate and ammonium in $PM_{2.5}$ in Chengdu, southwest China, based on 3-year measurements, Atmos. Chem. Phys., 20, 11181–11199, https://doi.org/10.5194/acp-20-11181-2020, 2020.

Le, T., Wang, Y., Liu, L., Yang, J., Yung, Y. L., Li, G., and Seinfeld, J. H.: Unexpected air pollution with marked emission reductions during the COVID-19 outbreak in China, Science, 369, 702–706, https://doi.org/10.1126/science.abb7431, 2020.

Le Quéré , C., Jackson, R. B., Jones, M. W., Smith, A. J. P., Abernethy, S., Andrew, R. M., De-Gol, A. J., Willis, D. R., Shan, Y. L., Canadell, J. G., Friedlingstein, P., Felix Creutzig, F., and Peters, G. P.: Temporary reduction in daily global CO_2 emissions during the COVID-19 forced confinement, Nat. Clim. Chang., 10, 647–653, https://doi.org/10.1038/s41558-020-0797-x, 2020.

Lelieveld, J., Klingmüller, K., Pozzer, A., Burnett, R. T., Haines, A., and Ramanathan, V.: Effects of fossil fuel and total anthropogenic emission removal on public health and climate, P. Natl. Acad. Sci., 116, 7192–7197, https://doi.org/10.1073/pnas.1819989116, 2019.

Liao, H., Chang, W., and Yang, Y.: Climatic effects of air pollutants over China: A review, Adv. Atmos. Sci., 32, 115–139, https://doi.org/10.1007/s00376-014-0013-x, 2015.

Li, L., Li, Q., Huang, L., Wang, Q., Zhu, A., Xu, J., Liu, Z., Li, H., Shi, L., Li, R., Azari, M., Wang, Y., Zhang, X., Liu, Z., Zhu, Y., Zhang, K., Xue, S., Ooi, M. C. G., Zhang, D., and Chan, A.: Air quality changes during the COVID-19 lockdown over the Yangtze River Delta Region: An insight into the impact of human activity pattern changes on air pollution variation, Sci. Total Environ., 732, 139282, https://doi.org/10.1016/j.scitotenv.2020.139282, 2020.

Liu, X., Easter, R. C., Ghan, S. J., Zaveri, R., Rasch, P., Shi, X., Lamarque, J.-F., Gettelman, A., Morrison, H., Vitt, F., Conley, A., Park, S., Neale, R., Hannay, C., Ekman, A. M. L., Hess, P., Mahowald, N., Collins, W., Iacono, M. J., Bretherton, C. S., Flanner, M. G., and Mitchell, D.: Toward a minimal representation of aerosols in climate models: description and evaluation in the Community Atmosphere Model CAM5, Geosci. Model Dev., 5, 709–739, https://doi.org/10.5194/gmd-5-709-2012, 2012.

Liu, Y., Hong, Y., Fan, Q., Wang, X., Chan, P., Chen, X., Lai, A., Wang, M., and Chen, X.: Source-receptor relationships for $PM_{2.5}$ during typical pollution episodes in the Pearl River Delta city cluster, China, Sci. Total Environ., 596, 194–206, https://doi.org/10.1016/j.scitotenv.2017.03.255, 2017.

Ramanathan, V., Crutzen, P. J., Kiehl, J. T., and Rosenfeld, D.: Aerosols, climate, and the hydrological cycle, Science, 294, 2119–2124, https://doi.org/10.1126/science.1064034, 2001.

Ren, L., Yang, Y., Wang, H., Zhang, R., Wang, P., and Liao, H.: Source attribution of Arctic aerosols and associated Arctic warming trend during 1980–2018, Atmos. Chem. Phys., 20, 9067–9085, https://doi.org/10.5194/acp-2020-3,2020.

Sharma, S., Zhang, M., Anshika, Gao, J., and Kota, S. H.: Effect of restricted emissions during Covid-19 on air quality in india, Sci. Total Environ., 728, 138878, https://doi.org/10.1016/j.scitotenv.2020.138878, 2020.

Shen, L., Zhao, T., Wang, H., Liu, J., Bai, Y., Kong, S., Zheng, H., Zhu, Y., and Shu, Z.: Importance of meteorology in air pollution events during the city lockdown for COVID-19 in Hubei Province, Central China, Sci. Total Environ., 754, 142227, https://doi.org/10.1016/j.scitotenv.2020.142227, 2021.

Shindell, D. T., Lamarque, J.-F., Schulz, M., Flanner, M., Jiao, C., Chin, M., Young, P. J., Lee, Y. H., Rotstayn, L., Mahowald, N., Milly, G., Faluvegi, G., Balkanski, Y., Collins, W. J., Conley, A. J., Dalsoren, S., Easter, R., Ghan, S., Horowitz, L., Liu, X., Myhre, G., Nagashima, T., Naik, V., Rumbold, S. T., Skeie, R., Sudo, K., Szopa, S., Takemura, T., Voulgarakis, A., Yoon, J.-H., and Lo, F.: Radiative forcing in the ACCMIP historical and future climate simulations, Atmos. Chem. Phys., 13, 2939–2974, https://doi.org/10.5194/acp-13-2939-2013, 2013.

Smith, C. J., Kramer, R. J., Myhre, G., Alterskjær, K., Collins, W., Sima, A., Boucher, O., Dufresne, J.-L., Nabat, P., Michou, M., Yukimoto, S., Cole, J., Paynter, D., Shiogama, H., O'Connor, F. M., Robertson, E., Wiltshire, A., Andrews, T., Hannay, C., Miller, R., Nazarenko, L., Kirkevåg, A., Olivié, D., Fiedler, S., Lewinschal, A., Mackallah, C., Dix, M., Pincus, R., and Forster, P. M.: Effective radiative forcing and adjustments in CMIP6 models, Atmos. Chem. Phys., 20, 9591–9618, https://doi.org/10.5194/acp-20-9591-2020, 2020.

Sulaymon, I. D., Zhang, Y., Hopke, P. K., Hu, J., Zhang, Y., Li, L., Mei, X., Gong, K., Shi, Z., Zhao, B., and Zhao, F.: Persistent high $PM_{2.5}$ pollution driven by unfavorable meteorological conditions during the COVID-19 lockdown period in the Beijing-Tianjin-Hebei region, China, Environ. Res., 198, 111186, https://doi.org/10.1016/j.envres.2021.111186, 2021.

Tian, H., Liu, Y., Li, Y., Wu, C., Chen, B., Kraemer, M. U. G., Li, B., Cai, J., Xu, B., Yang, Q., Wang, B., Yang, P., Cui, Y., Song, Y., Zheng, P., Wang, Q., Bjornstad, O. N., Yang, R., Grenfell, B. T., Pybus, O. G., and Dye, C.: An investigation of transmission control measures during the first 50 days of the COVID-19 epidemic in China, Science, 368, 638–642, https://doi.org/10.1126/science.abb6105, 2020.

UCAR: CAM5 model, UCAR [code], available at: http://www.cesm.ucar.edu/models/cesm1.2/, last access: 14 October 2021.

Vautard, R., Yiou, P., and Oldenborgh, G.: Decline of fog, mist and haze in Europe over the past 30 years, Nat. Geosci., 2, 115–119, https://doi.org/10.1038/ngeo414, 2009.

Wang, H., Easter, R. C., Rasch, P. J., Wang, M., Liu, X., Ghan, S. J., Qian, Y., Yoon, J.-H., Ma, P.-L., and Vinoj, V.: Sensitivity of remote aerosol distributions to representation of cloud–aerosol interactions in a global climate model, Geosci. Model Dev., 6, 765–782, https://doi.org/10.5194/gmd-6-765-2013, 2013.

Wang, H., Rasch, P. J., Easter, R. C., Singh, B., Zhang, R., Ma, P. L., Qian, Y., Ghan, S. J., and Beagley, N.: Using an explicit emission tagging method in global modeling of source-receptor relationships for black carbon in the Arctic: Variations, sources, and transport pathways, J.-Geophys. Res., 119, 12888–12909, https://doi.org/10.1002/2014JD022297, 2014.

Wang, H., Easter, R. C., Zhang, R., Ma, P., Singh, B., Zhang, K., Ganguly, D., Rasch, P. J., Burrows, S. M., Ghan, S. J., Lou, S., Qian, Y., Yang, Y., Feng, Y., Flanner, M., Leung, L. R., Liu, X., Shrivastava, M., Sun, J., Tang, Q., Xie, S., and Yoon, J.: Aerosols in the E3SM Version 1: New Developments and Their Impacts on Radiative Forcing, J. Adv. Model. Earth Sy., 12, 293, https://doi.org/10.1029/2019MS001851, 2020.

Wang, P., Chen, K., Zhu, S., Wang, P., and Zhang, H.: Severe air pollution events not avoided by reduced anthropogenic activities during COVID-19 outbreak, Resour. Conserv. Recycl., 158, 104814, https://doi.org/10.1016/j.resconrec.2020.104814, 2020.

Wang, Q., Huang, R. J., Cao, J., Tie, X., Shen, Z., Zhao, S., Han, Y., Li, G., Li, Z., Ni, H., Zhou, Y., Wang, M., Chen, Y., and Zhou, Y.: Contribution of regional transport to the black carbon aerosol during winter haze period in Beijing, Atmos. Environ., 132, 11–28, https://doi.org/10.1016/j.atmosenv.2016.02.031, 2016.

Watson, J. G.: Visibility: Science and regulation, J. Air Waste Manage. Assoc., 52, 628–713, https://doi.org/10.1080/10473289.2002.10470813, 2002.

Xu, Q., Wang, S., Jiang, J., Bhattarai, N., Li, X., Chang, X., Qiu, X., Zheng, M., Hua, Y., and Hao, J.: Nitrate dominates the chemical composition of $PM_{2.5}$ during haze event in Beijing, China, Sci. Total Environ., 689, 1293–1303, https://doi.org/10.1016/j.scitotenv.2019.06.294, 2019.

Xue, W. B., Fu, F., Wang, J. N., Tang, G. Q., Lei, Y., Yang, J. T., and Wang, Y. S.: Numerical study on the characteristics of regional transport of $PM_{2.5}$ in China, J. Environ. Sci., 34, 1361–1368, 2014.

Yang, Y., Wang, H., Smith, S. J., Ma, P. L., and Rasch, P. J.: Source attribution of black carbon and its direct radiative forcing in China, Atmos. Chem. Phys., 17, 4319–4336, https://doi.org/10.5194/acp-17-4319-2017, 2017a.

Yang, Y., Wang, H., Smith, S. J., Easter, R., Ma, P. L., Qian, Y., Yu, H., Li, C., and Rasch, P. J.: Global source attribution of sulfate concentration and direct and indirect radiative forcing, Atmos. Chem. Phys., 17, 8903–8922, https://doi.org/10.5194/acp-17-8903-2017, 2017b.

Yang, Y., Wang, H., Smith, S. J., Zhang, R., Lou, S., Qian, Y., Ma, P.-L., and Rasch, P. J.: Recent intensification of winter haze in China linked to foreign emissions and meteorology, Sci. Rep., 8, 2107, https://doi.org/10.1038/s41598-018-20437-7, 2018a.

Yang, Y., Wang, H., Smith, S. J., Easter, R. C., and Rasch, P. J.: Sulfate aerosol in the Arctic: Source attribution and radiative forcing, J.-Geophys. Res., 123, 1899–1918, https://doi.org/10.1002/2017JD027298, 2018b.

Yang, Y., Wang, H., Smith, S. J., Zhang, R., Lou, S., Yu, H., Li, C., and Rasch, P. J.: Source apportionments of aerosols and their direct radiative forcing and long-term trends over continental United States, Earth's Future, 6, 793–808, https://doi.org/10.1029/2018EF000859, 2018c.

Yang, Y., Smith, S. J., Wang, H., Mills, C. M., and Rasch, P. J.: Variability, timescales, and nonlinearity in climate responses to black carbon emissions, Atmos. Chem. Phys., 19, 2405–2420, https://doi.org/10.5194/acp-19-2405-2019, 2019a.

Yang, Y., Smith, S. J., Wang, H., Lou, S., and Rasch, P. J.: Impact of anthropogenic emission injection height uncertainty on global sulfur dioxide and aerosol distribution, J.-Geophys. Res., 124, 4812–4826, https://doi.org/10.1029/2018JD030001, 2019b.

Yang, Y., Lou, S., Wang, H., Wang, P., and Liao, H.: Trends and source apportionment of aerosols in Europe during 1980–2018, Atmos. Chem. Phys., 20, 2579–2590, https://doi.org/10.5194/acp-20-2579-2020, 2020.

Yang, Y.: Data for Aerosol transport pathways and source attribution in China during the COVID-19 outbreak, Zenodo [data set], https://doi.org/10.5281/zenodo.5564726, 2021.

Yu, H., Remer, L. A., Chin, M., Bian, H., Kleidman, R. G., and Diehl, T.: A satellite-based assessment of transpacific transport of pollution aerosol, J.-Geophys. Res., 113, D14S12, https://doi.org/10.1029/2007JD009349, 2008.

Yu, H. B., Remer, L. A., Chin, M., Bian, H. S., Tan, Q., Yuan, T. L., and Zhang, Y.: Aerosols from overseas rival domestic emissions over North America, Science, 337, 566–569, https://doi.org/10.1126/science.1217576, 2012.

Zhang, R., Wang, H., Hegg, D. A., Qian, Y., Doherty, S. J., Dang, C., Ma, P.-L., Rasch, P. J., and Fu, Q.: Quantifying sources of black carbon in western North America using observationally based analysis and an emission tagging technique in the Community Atmosphere Model, Atmos. Chem. Phys., 15, 12805–12822, https://doi.org/10.5194/acp-15-12805-2015, 2015.

Zheng, B., Tong, D., Li, M., Liu, F., Hong, C., Geng, G., Li, H., Li, X., Peng, L., Qi, J., Yan, L., Zhang, Y., Zhao, H., Zheng, Y., He, K., and Zhang, Q.: Trends in China's anthropogenic emissions since 2010 as the consequence of clean air actions, Atmos. Chem. Phys., 18, 14095–14111, https://doi.org/10.5194/acp-18-14095-2018, 2018.

Zhu, J., Xia, X., Che, H., Wang, J., Zhang, J., and Duan, Y.: Study of aerosol optical properties at Kunming in southwest China and longrange transport of biomass burning aerosols from North Burma, Atmos. Res., 169, 237–247, https://doi.org/10.1016/j.atmosres.2015.10.012, 2016.

Zhu, J., Xia, X., Wang, J., Zhang, J., Wiedinmyer, C., Fisher, J. A., and Keller, C. A.: Impact of Southeast Asian smoke on aerosol properties in Southwest China: First comparison of model simulations with satellite and ground observations, J. Geophys. Res.-Atmos., 122, 3904–3919, https://doi.org/10.1002/2016JD025793, 2017.